Journal of Hydroscience and Hydraulic Engineering
Vol. 19, No.2 November, 2001, 105-117

INTERNAL WIND WAVES AND SNOW CLOUDS ON A MOUNTAIN SLOPE

By

Keisuke Nakayama

Marine Environment Division,
National Institute for Land and Infrastructure Management,
Nagase 3-1-1, Yokosuka, Japan

and

Daisaku Saitoh

Ministry of Land, Infrastructure and Transport,
Sapporo, Japan

SYNOPSIS

In Japan, there are many mountains that have steep slopes which cause wind fields to change and have an effect on rain and snowfall. These effects are very complicated due to atmospheric stratification. One of the effects of stratification in numerical computations is that a wind direction inversion layer may occur in front of the mountain slope when humidity is very low. On the contrary, stratification can change into a neutral state if humidity becomes high and cloud microphysical processes are taken into account, as air releases latent heat. In the case where humidity is appropriately given, a cold air current is caused in front of the mountain and snow clouds appear on top of the cold air current (Nakayama et al, 1998). This phenomena will be referred to as SCAC (Snow Clouds on top of the Cold Air Current) hereafter. The purpose of this study is to determine the effects of internal wind waves caused by a sin-curved mountain in front of a second steep and long slope by using an Advanced Regional Prediction System (ARPS). As a result, it is revealed that snow clouds appear on top of the cold air current and mountains play a role in the decreasing amounts of snowfall.

INTRODUCTION

Japan is a country with many steep sloped mountains, and they have an effect on wind fields, rain, and snowfall. Because of the interactions between wind fields and microphysics of cloud, it is thought that these phenomena are very complicated and internal waves in a stratified field can occur.

Previous studies of rainfall and snowfall over an isolated mountain with internal waves have been; (1) numerical analysis on internal waves caused by an isolated mountain with a dry atmosphere (Saitoh et al, 1998); (2) numerical simulation for the influence of the internal waves with an isolated mountain on the extention of snowfall area (Nakayama et al, 1998).

If the wavelength of an isolated mountain is consistent with that of an internal

wave, the area of snowfall extends. However, their studies are concerned with the effects of an isolated mountain and do not consider the interactions between mountains. On the other hand, on a long and steep slope, it is possible that the shear layer near the surface occurs because momentum is not enough to flow uniformly over the vertical axis of the slope.

In Japan, there are numerous mountains whose shape can be assumed to be a sin-curve, due to their steep and long slopes, in particular, isolated mountains. Isolated mountains and mountain ranges in front of a second steep and long slope cause internal waves and their reflections tend to occur on the second slope. That is to say, internal waves caused on the leeward side of an isolated mountain may have a considerable effect on a wind field in front of the second slope.

Previous studies related to the effects of internal waves on a long slope may be summarized as follows: 1) experiments in a stratified field were conducted to obtain a mixing ratio caused by the reflection of internal waves (Silvia et al, 1997), 2) internal waves breaking over a slope (Timothy et al, 1985), and 3) vertical mixing due to the breaking of critical internal waves on sloping boundaries (Ivey, 1989). Attention was paid to the mixing over a slope caused by internal aquatic waves in limnology and oceanography, which gives us useful information about flow in a stratified field. However, because of microphysical processes, it appears that a wind field is more complicated in the atmosphere. For example, snow clouds form due to the interaction between isolated mountain slopes as cold air currents due to stratification cause an ascending wind on top of a front and it does not occur where the front is located.

In this study, an isolated mountain that has a sin-curved shape is located in front of a second long and steep slope, and the isolated mountain causes internal waves. This study aims to understand the effects of isolated mountains on the mixing of internal waves, and to investigate snow clouds on top of a front of cold air currents due to stratification.

WIND INVERSION LAYER OVER A SLOPE IN A STRATIFIED FLOW FIELD

Three dimensional numerical simulations were carried out by using an Advanced Regional Prediction System (ARPS). The characteristics of this model are that fluid is compressible and non-hydrostatic pressure is used. The first order large eddy simulation by Deardorff is used (Deardorff, 1975; Tal et al, 1993).

Figure 1 shows a schematic diagram of the computational domain. The number of grid points are 125x 25 horizontally and 30 vertically. The grid intervals are uniform, 500 m, horizontally, and vertically increase from 50 m from the ground/sea surface to 250 m at the upper wall. The height of the upper wall is given as 4.5 km since cumulus convection energy is small compared with that of the equator in the northern part of Japan. Other conditions related to topography are shown as follows: the Brunt-Vaisala frequency N is constant 0.01 1/s, and the horizontal velocity U is uniform 10 m/s in the vertical axis. The height of the slope H is 1,000 m, and the length of the slope Lu is 15,000 m. The height of the isolated mountain hs is 0 m, and d+l/2=25,000 m. In this chapter's simulation, we do not include microphysical processes.

In the case where the wind flows over a second long and great slope in a stratified field, it is expected that the wind near the surface cannot flow over the slope and that a wind inversion layer could be caused. Therefore, the flow can be divided into two regions bellow and over the wind inversion layer. As the shear layer has an enormous amount of turbulence, it affects the occurrence of snow clouds. This could provide useful data as to the height of the shear layer.

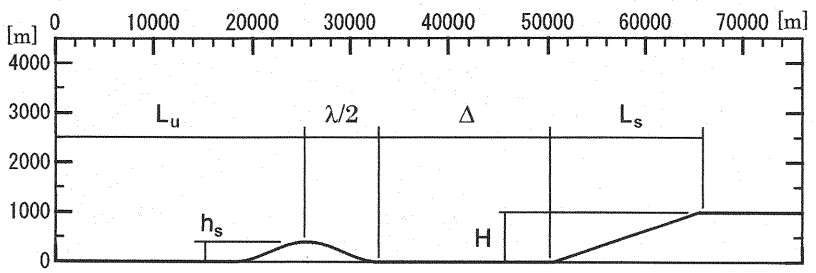

Figure 1 Schematic of the computational domain

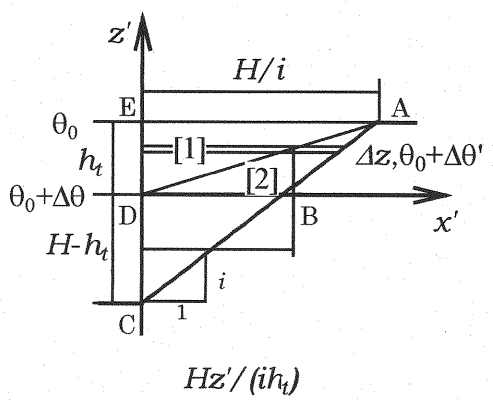

Figure 2 Schematic diagram from around a shear layer

Figure 2 shows a schematic diagram used to analyze the shear layer. The depth from the wind inversion layer to the top of the slope is ht and the Brunt-Vaisala frequency is given to be constant in a vertical coordinate. Momentum to raise the air in section [1] is obtained by equation (1).

$$M_1 = \int_0^{h_t} \rho_0 \frac{\Delta\theta'}{\theta_0} g(h_t - z') \frac{Hz'}{ih_t} dz' = \rho_0 g H h_t^2 \frac{\Delta\theta}{12\theta_0 i} \qquad (1)$$

When the wind flows constantly with the velocity U at the height of the slope (m/s), vertical momentum in section (1) is obtained by using a slope equation (2). Velocity at point A and D is equal to zero, and velocity at point E is equal to U.

$$M_2 = \int_0^{h_t} \int_0^{\frac{Hz}{ih_t}} \rho_0 \left(U \frac{z'}{h_t} \frac{Hz'/ih_t - x'}{Hz'/ih_t} \right)^2 i dx' dz' = \rho_0 U^2 \frac{H h_t}{12} \qquad (2)$$

The area where an ascending wind occurs is derived under the condition that M2 is greater than M1. The difference of temperature between A and D is given as equation (4) by using the Brunt-Vaisala number and the depth of the shear layer was obtained by equation (3).

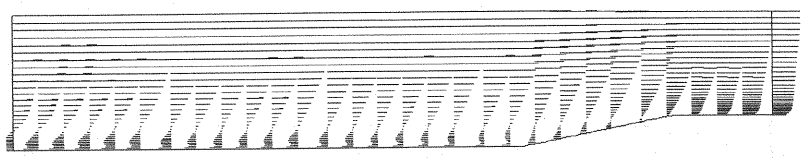

10 m/s

Figure 3 Velocity vector in a longitudinal plane at 14400 sec after the beginning of the computation

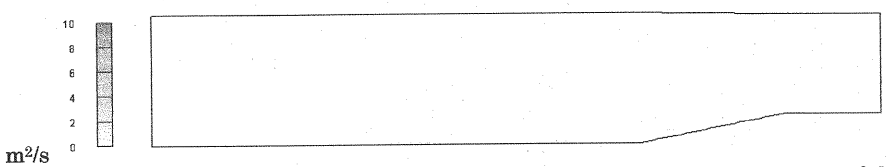

Figure 4 Eddy viscosity in a longitudinal section at 14400 sec after the beginning of the computation

$$M_1 \leqq M_2 \tag{3}$$

$$h_t \leqq \sqrt{i}\,\frac{U}{N} \tag{4}$$

$$\because \Delta\theta = \frac{\theta_0}{g} N^2 h_t$$

In cases where i, U and N are equal to 1/15, 4 m/s and 0.005 1/s, respectively, ht becomes equal to 207 m by using equation (3).

To compare the theoretical solution (3) with the numerical simulation, we carried out the computation under the same conditions. Figure 3 shows the velocity vector at 14400 (seconds) after the beginning of the computation when the wind vector is in a stable state. The air cannot flow over the bottom of the slope, as winds descend along the slope due to stratification. In this computation, ht is about 250 m and is almost consistent with the theoretical solution, equation (3).

In section [2], we assume that the streamline along the slope is parallel to the slope. Based on this assumption, horizontal velocity between C and D is obtained as equation (5) by using the Berounuis-law. The theoretical solution for us was found to be 3.63 m/s when Dt is 0.719 K. The computation result was 4.0 m/s and consistent with the theoretical one.

$$u_s(z') = \left(-2g \frac{\Delta\theta}{(1+i^2)\theta_0} \frac{h_t}{H - h_t} z' \right)^{1/2} \tag{5}$$

Figure 4 and 5 show the distribution of eddy viscosity and vertical velocity at 14400 sec respectively after the beginning of the computation. Eddy viscosity is greater near the slope and causes turbulence in the atmosphere. Ascending and descending currents occur mutually in the wind field. The interval of the ascending and the descending currents become less near the slope where the turbulence is greatest.

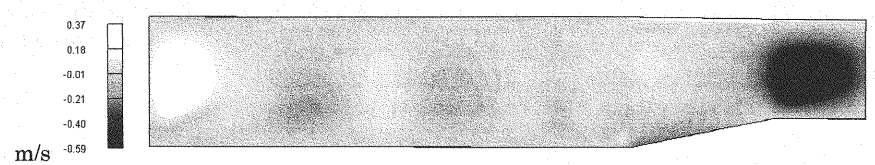

Figure 5 Vertical velocity in a longitudinal section at 14400 sec after the beginning of the computation

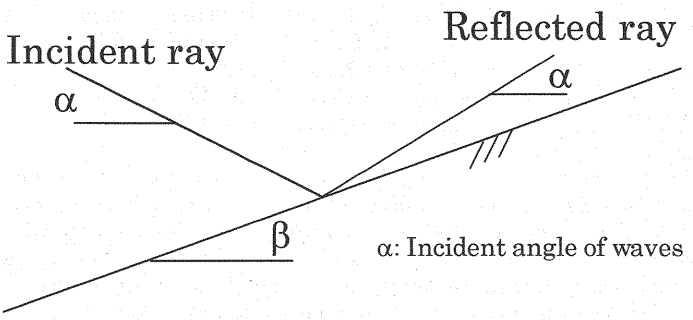

Figure 6 Schematic diagram of an internal wave reflecting on a sloping bed

THE EFFECTS OF AN ISOLATED MOUNTAIN SLOPE IN FRONT OF A SECOND MOUNTAIN SLOPE WITHOUT MICROPHISICAL PROCESSES

To clarify the effects of an isolated mountain slope in front of a second mountain slope; numerical simulations were carried out by changing l, and the width of the mountain skirt. The depth of the shear layer (ht), is estimated at about 300 m in the numerical simulation, where hs is given at 400 m, which is half the height from the flat boundary to the shear layer.

A previous study indicates that internal waves on the slope are classified by the relationship of Brunt-Vaisala frequencies 3). Figure 6 shows a schematic diagram indicating the relationship between an internal wave and the reflection over a slope. Equation (6) shows a critical number that is super critical when g is greater than 1.0 and under critical when g is less than 1.0.

$$\gamma = \omega/\omega_c \tag{6}$$

$$\omega = 2\pi\frac{U}{\lambda} \tag{7}$$

$$\frac{\omega}{N} \leqq 1 \tag{8}$$

where, b = slope.

In this study, as the slope of the second slope is given tan-1(H/Ls)=0.0666p, l is derived 94,500 m for equation (6) when g is 1.0. In Japan, there are few isolated mountains with such a long skirt; therefore most cases are included in the super critical. The condition indicated by equation (9) is necessary to cause an internal wave; therefore computations were carried out under the condition, 6,280 m < l < 94,500 m. Table 1

shows the condition for the computation. Lu indicates the distance from the windward to the center of the isolated mountain and l/2+d is constant as the analysis revealed in the previous chapter.

$$\omega_c = N \sin\beta \quad . \tag{9}$$

Table 1 Conditions for numerical simulations

	Lu	λ	Δ	γ
Case 1	25,000m	7,000m	21,500m	13.5
Case 2	25,000m	10,000m	15,000m	9.45
Case 3	25,000m	15,000m	17,500m	6.30
Case 4	25,000m	20,000m	15,000m	4.72
Case 5	25,000m	30,000m	10,000m	3.15
Case 6	25,000m	40,000m	5,000m	2.36

Figure 7 shows eddy viscosity from the center of the isolated mountain slope to the end of the second slope shown from case 1 to case 6 at 18,000 sec after the beginning of the computation. In case 1, as the internal wave length is consistent with the length of the skirt of the isolated mountain, eddy viscosity becomes greater around the shear layer than other cases due to resonance. In case 2 and case 3, eddy viscosity is smaller than case 1 because the width of the isolated mountain is longer than the internal wavelength. But, in case 4 to case 6, eddy viscosity becomes greater than case 2 and case 3.

Figure 8 shows vertical velocity in the same area as figure 7 from case 1 to case 6. The absolute velocity on the second slope decreases gradually from case 1 to case 4. The result is that the resonance is inhibited, like eddy viscosity. However, an ascending current over the second slope increases gradually from case 5 to case 6.

The results of these computations are related to the steepness indicated by equation (10). The steepness of the wavelength of the isolated mountain decreases from case 1 to case 6. As the slope increases so does the amount of energy lost. Therefore, in case 3, the shear layer cannot be completely caused by the great steepness and resonance of the internal waves.

$$\Gamma \approx \frac{h_s}{\lambda} \tag{10}$$

Where, g is steepness of the mountain.

In case 6, the reason why the eddy viscosity is great is as follows: as the length of the skirt of the isolated mountain is greater than the length of the second slope, it would appear that there are no breaking waves and less energy is dissipated.

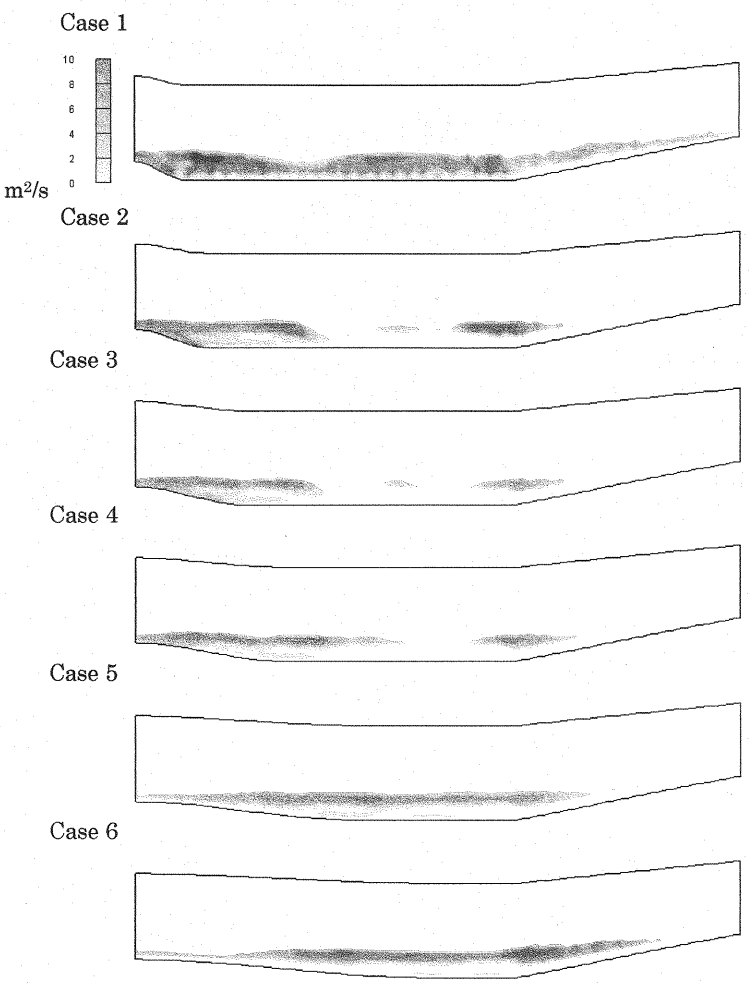

Figure 7 Eddy viscosity in a longitudinal plane from case 1 to case 6

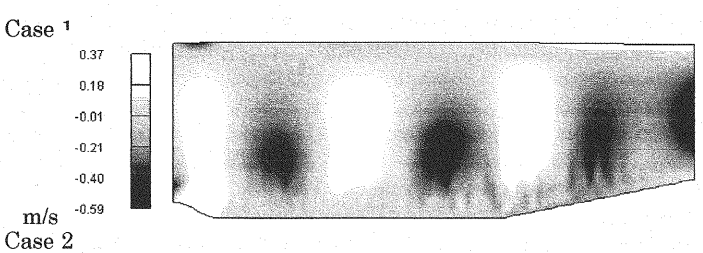

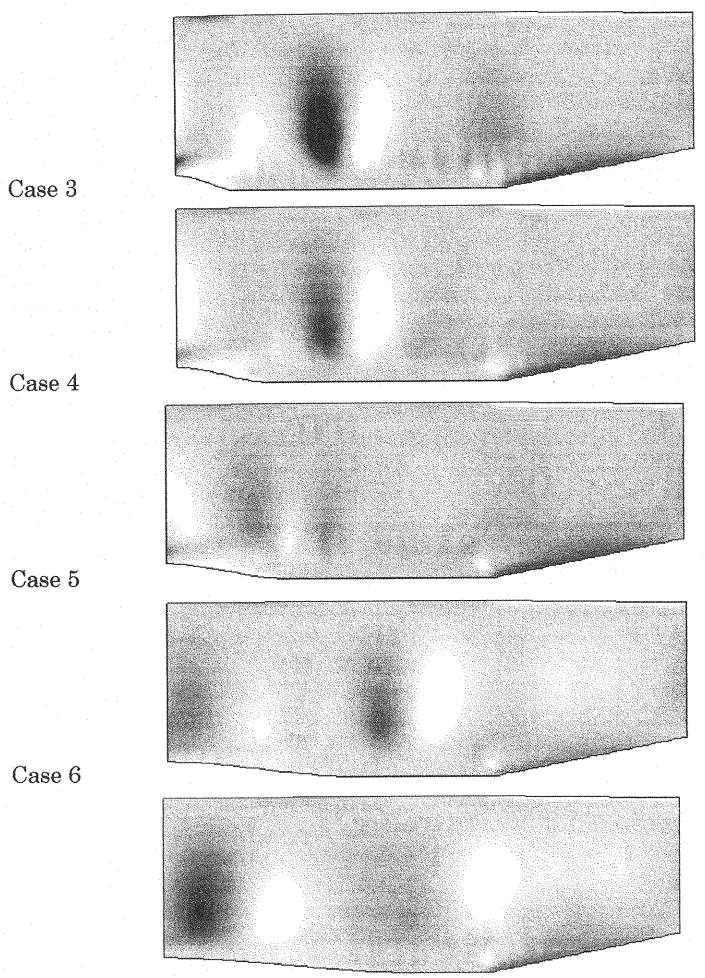

Figure 8 Vertical velocity in a longitudinal plane from case 1 to case 6

THE EFFECTS OF AN ISOLATED MOUNTAIN SLOPE IN FRONT OF A SECOND SLOPE WITH MICROPHISICAL PROCESSES

In the next stage of this study, we carried out the same computation as case 1, case 4 and case 6 but with microphysical processes, because these three cases have different conditions with respect to resonance and steepness. Relative humidity was given at 90% when snow clouds easily occur. The Brunt-Vaisala frequency was given at N=0.01 1/s by considering the humidity.

Figure 9 shows a velocity vector and vertical velocity with the snow-mixing ratio in the absence of an isolated mountain. The velocity vector is much different from figure 3 and is similar to the potential flow because there is no wind inversion layer near the surface and the velocity on top of the second slope is greater than the velocity on the bottom of the second slope. Latent heat is released when atmospheric vapor

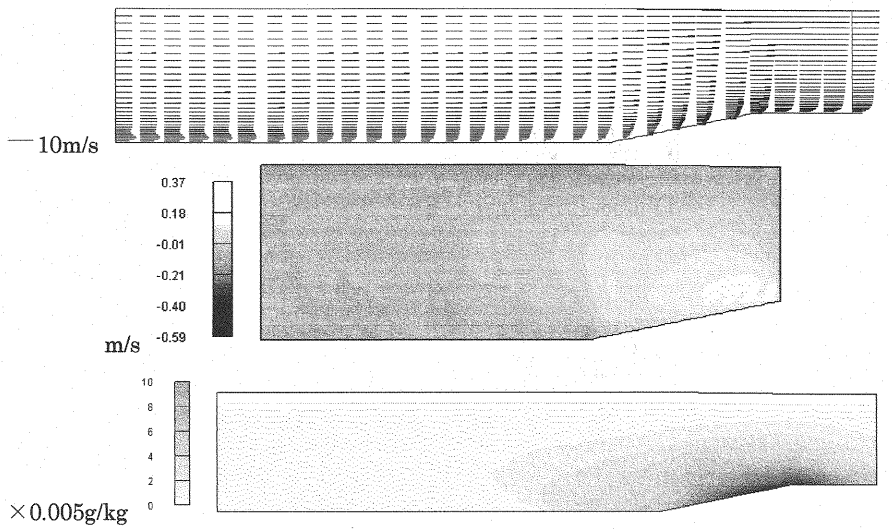

Figure 9 Velocity vector: vertical velocity and the snow-mixing ratio in a longitudinal plane at 18000 sec after the beginning of the computation, while taking into account microphysical processes

forms snow clouds, and the Brunt-Vaisala frequency causes a decrease due to the occurrence of shear layers over the second slope. As there is no wind inversion layer, the great ascending current occurs on top of the second slope.

Figure 10 shows vertical velocity in case 1, case 4 and case 6. The wavelength of the internal wave is smaller than that of figure 8 because of great ascending and descending currents, which occur due to releasing latent heat. Due to the long wavelength a breaking wave could not occur in case 6 without microphysical processes (figure 8), it appears that the breaking waves occur over the second slope due to the increase in wave frequency (figure 10). For example, in case 4, the breaking waves do not occur as shown figure 8, because there is a little fluctuation of vertical currents over the second slope. However, in figure 10, the fluctuation of vertical currents is greater than that of figure 8 and it is clear that breaking waves occur on the second slope.

Figure 11 shows a snow-mixing ratio at 18,000 sec. The shorter the length of the skirt of the isolated mountain, the more the center of the snow cloud moves windward. Furthermore, the maximum snow-mixing ratio decreases from case 1 to case 6 gradually. In the case where the numerical simulation without microphysical processes, it was expected that the snow-mixing ratio would become greater due to the increase in ascending and descending currents. When the length of the skirt of the isolated mountain is consistent with the internal wavelength, or when the width of the isolated mountain becomes greater than the length of the second slope, a strong ascending wind occurs on the second slope. However, in the case of the numerical simulation with microphysical processes, the internal waves play a role in decreasing the snow-mixing ratio, as the slope decreases, and therefore the snow-mixing ratio becomes lower.

Findings show that a shear layer occurs under dry conditions and snow clouds occur over a second mountain slope under the 100% humidity. The temperature difference under the shear layer is due to the initial condition being less than zero and the area under the shear layer is considered as a cold air current. Previous studies with

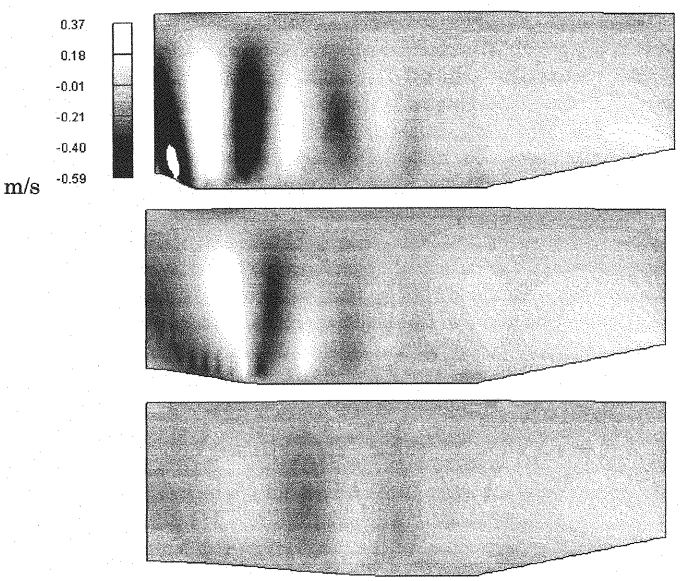

Figure 10 Vertical velocity in a logitudinal plane in case 1, case 4 and case 6

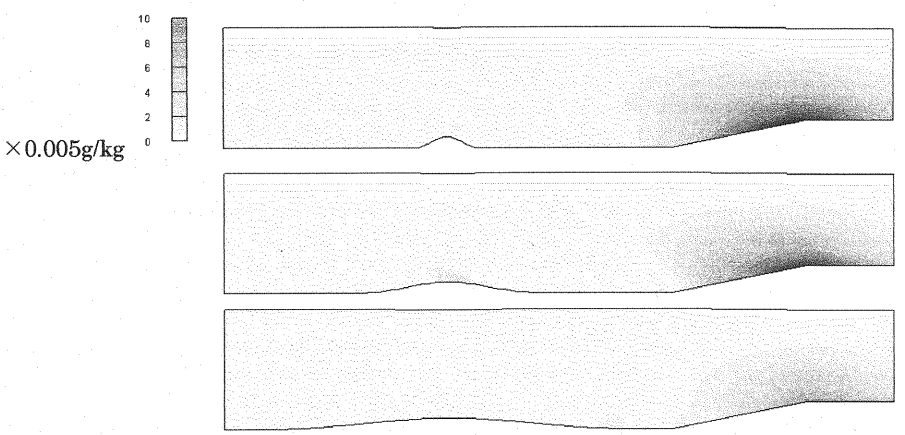

Figure 11 Snow mixing ratio in a logitudinal plane in case 1, case 4 and case 6

respect to cold air currents found that radiative cooling causes SCAC, and that snow clouds on a line of discontinuity are caused by mutual interference of an air current (Tsuboki et al, 1989; Fujiyoshi et al, 1996). But they do not consider the shear layer in a stratified flow field.

The stratified field under dry conditions causes a back current on long and steep slopes and an increase in the relative humidity plays a role in suppressing a back current. It is possible to represent a cold air current and snow clouds by giving an adequate Brunt-Vaisala frequency and relative humidity. Figure 12 shows the initial

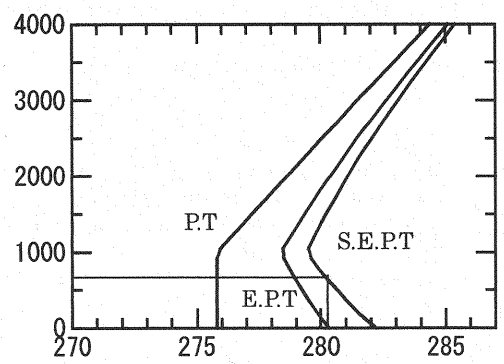

Figure 12 Initinal condition for the computation.
Solid lines indicate potential temperature (P.T.), equivalent potential temperatures (E.P.T) and saturation equivalent potential temperatures (S.E.P.T.) from the left to right side of the figure.

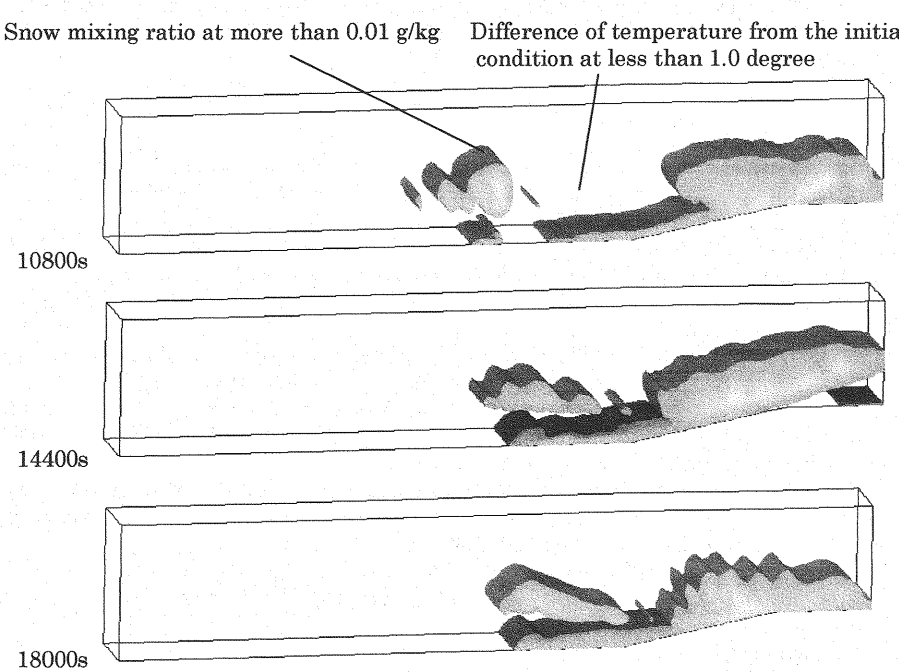

Figure 13 Snow mixing ratio (more than 0.10 g/kg) and a cold air current where the decrease in temperature is 1.0 degree at 10800 sec to 18000 sec.

conditions for the numerical simulation represented by cold air currents and snow clouds. It is apparent that snow clouds form easily because (LFC) is about 600 m and the theoretical solution for H-ht is about 700 m.

Figure 13 shows the time series of the snow-mixing ratio, more than 0.10 g/kg and the difference of temperature below 1.0 from the initial condition. At 10,800 sec

after the beginning of the computation, a cold air current is formed in front of the second slope and SCAC appears. At 18,000 sec after the beginning of the computation, snow clouds formed clearly over the cold air current.

CONCLUSIONS

(1) The height from the shear layer to the top of the slope and the velocity in the back current are obtained theoretically under the condition that the upper wind is uniform and the Brunt-Vaisala frequency is constant. They are consistent with those of the numerical simulation results.

(2) In Japan, g is greater than 1.0 generally. In the case without microphysical processes, turbulence becomes greatest when the length of the skirt of the isolated mountain is consistent with the internal wavelength, or when the width of the isolated mountain is greater than the length of the second slope.

(3) In the case with microphysical processes, flow fields are similar to potential flow because the release of latent heat inhibits the occurrence of the shear layer.

(4) In the case where microphysical processes, it was found that the isolated mountain plays a large role in the formation of snow clouds. The snow-mixing ratio decreases when the length of the skirt of the isolated mountain is greatest.

(5) SCAC occurs when there is adequate radative humidity, Brunt-Vaisala frequency and velocity.

REFERENCES

1. Deardorff, J.: The development of boundary-layer turbulence models for use in studying the severe storm environment, Proc. SESAME Meeting, Boulder, NOAA-ERL, pp.251-264, 1975.
2. Fujiyoshi, Y., Y. Kodama, K. Tsuboki, K. Nishimura and N. Ono: Structure of Cold Air During the Development of a Broad Band Cloud and a Meso-scale Vortex; Simultaneous Two-Point Radiosonde Observations, Journal of the Meteorological Society of Japan, Vol.74, pp.281-297, 1996.
3. IVEY, G.N. and R.I. NOKES: Vertical mixing deu to the breaking of critical internal waves on sloping boundaries, J.Fluid Mech., vol.204, pp.479-500, 1989.
4. Nakayama, K., K. Hasegawa and M. Fujita: A study on the shape of a cold air flow around Ishikari bay in winter at a vertical plane, Annual journal of hydraulic engineering, JSCE, Vol.39, pp.177-182, 1995.
5. Nakayama, K., K. Hasegawa and M. Fujita: A Numerical Study on a Cold Air Flow Which Causes Snow Clouds Around Sapporo City, Annual journal of hydraulic engineering, JSCE, Vol.41, pp.129-134, 1997.
6. Nakayama, K., K. Hasegawa and M. Fujita: Analysis of cold air flow with snow cloud in Ishikari bay, Journal of hydraulic, coastal and environmental engineering, No.539, pp.31-42, 1997.
7. Nakayama, K., K. Hasegawa and M. Fujita: Structures of Snow Clouds Associated with a Cold Air Flow, Journal of hydraulic, coastal and environmental engineering, No.593, pp.1-10, 1998.
8. Nakayama, K. and R. Hatabata: The influence of internal waves on the snowfall area, The conference of Hydrology and Water Resources, p.251, 1998.
9. Saitoh, K, G. Doma, U. Schaettler and J. Steppeler: 3-D Mountain Waves by the Lokal-Modell of DWD and the MRI Mesoscale Nonhydrostatic Model, Pap. Met. Geophys., 49, pp.7-19, 1998.
10. Silva, I.P.D.DE, J. Imberger and G.N. Ivey: Localized mixing due to a breaking internal wave, J.Fluid Mech., vol.350, pp.1-27, 1997.

11. Tao, W.K. and J. Simpson: Goddard cumulus ensemble model. Part 1: Model description, Terrestrial, Atmospheric and Oceanic Sciences, Vol.4, pp.35-72, 1993.
12. Timothy, W. Kao, F.S. Pan and D. Renouard: Internal solitons on the pycnocline: generation, propagation, and shoaling and breaking over a slope, J.Fluid Mech., vol.159, pp.19-53, 1985.
13. Tsuboki, K., Y. Fujiyoshi and G. Wakahama: Structure of a Land Breeze and Snowfall Enhancement at the Leading Edge, Journal of the Meteorological Society of Japan, pp.757-769, 1989.

(Received August 30, 2000 ; revised June 14, 2001)